Colloids and Surfaces B: Biointerfaces 253 (2025) 114754

Contents lists available at ScienceDirect

Colloids and Surfaces B: Biointerfaces

journal homepage: www.elsevier.com/locate/colsurfb

Delivery of *Ulva rigida* extract by bicontinuous cubic lipid nanoplatforms for potential photodynamic therapy against pancreatic cancer

Karolina Krautforst [a,b,c], Julita Kulbacka [d,e], Marco Fornasier [c,f], Rita Mocci [a], Debora Dessì [g], Andrea Porcheddu [a], Davide Moccia [g], Antonio Pusceddu [g], Giorgia Sarais [g], Sergio Murgia [c,g,*], Urszula Bazylińska [b,**]

[a] Department of Chemical and Geological Sciences, University of Cagliari, s.s. 554 bivio Sestu, Monserrato, CA I-09042, Italy
[b] Department of Physical and Quantum Chemistry, Faculty of Chemistry, Wroclaw University of Science and Technology, Wybrzeze Wyspianskiego 27, Wroclaw 50-370, Poland
[c] CSGI, Consorzio Interuniversitario per lo Sviluppo dei Sistemi a Grande Interfase, via della Lastruccia 3, 50019 Sesto Fiorentino, Florence, Italy
[d] Department of Molecular and Cellular Biology, Faculty of Pharmacy, Wroclaw Medical University, Borowska 211 A, Wroclaw 50-556, Poland
[e] Department of Immunology and Bioelectrochemistry, State Research Institute Centre for Innovative Medicine Santariškių g. 5, Vilnius LT-08406, Lithuania
[f] Department of Chemistry, Lund University, Lund SE-22100, Sweden
[g] Department of Life and Environmental Sciences, University of Cagliari, s.s. 554 bivio Sestu, Monserrato, CA I-09042, Italy

ARTICLE INFO

Keywords:
Marine algae
Microwave-assisted extraction
Lipid liquid crystalline nanocarriers
Cubosomes
Natural photosensitizers
BxPC-3 cells
Anticancer activity

ABSTRACT

Ulva rigida is a widely available marine algae representing a valuable biomass from which natural photosensitizers (chlorophylls) can be obtained in an environmentally friendly manner using a green microwave-assisted extraction technique. If properly loaded in biocompatible nanoformulations, such highly hydrophobic chlorophylls with photosensitizing activity may constitute effective drugs useful in photodynamic therapy (PDT) against extremely resistant pancreatic cancer cells. To permit adequate solubilization in water, prevent immune system activation, and improve pharmacokinetic properties, an extract from *Ulva rigida* biomass was encapsulated in two monoolein-based cubosome formulations differing for the dispersants used for their stabilization in water: Pluronic F108 (CUB) or a mixture of sorbitan monooleate and sodium taurocholate (TS-CUB). In both cases, high encapsulation efficiency was achieved. The formulations were investigated from a physicochemical point of view (SAXS, cryo-TEM, DLS, ELS), and the production of reactive oxygen species was evaluated. In addition, an extensive evaluation of biocompatibility and bioactivity was conducted on the human pancreatic cancer cell line BxPC-3. This assessment included an MTT cytotoxicity assay, cellular uptake analysis via flow cytometry, and cytoskeleton imaging both under dark conditions and post-irradiation to evaluate the effects of PDT. Unloaded nanoparticles were characterized by an inner bicontinuous cubic phase (Pn3m). However, after encapsulation of the *Ulva rigida* extract the presence of a sponge phase (L3) in the TS-CUB formulation was observed. Compared with CUB, TS-CUB loaded with the extract demonstrated enhanced photoactivity, superior biocompatibility, and more potent *in vitro* anticancer activity against pancreatic cancer through photodynamic therapy (PDT).

1. Introduction

Marine algae contain a wide spectrum of different bioactive molecules, due to metabolic activity adapted to different and often harsh environmental conditions [1]. Among all components of the green algae biomass, an interesting group is represented by the pigments known as chlorophylls [2,3]. Due to their porphyrin ring structure, these hydrophobic molecules are recognized as potent natural photosensitizers (PSs). In addition, chlorophylls are highly efficient at generating reactive oxygen species (ROS) when exposed to red light [4]. This property

* Corresponding author at: CSGI, Consorzio Interuniversitario per lo Sviluppo dei Sistemi a Grande Interfase, Sesto Fiorentino, via della Lastruccia 3, 50019, Florence, Italy.
** Corresponding author at: Department of Physical and Quantum Chemistry, Faculty of Chemistry, Wroclaw University of Science and Technology, Wybrzeze Wyspianskiego 27, Wroclaw 50-370, Poland.
E-mail addresses: murgias@unica.it (S. Murgia), urszula.bazylinska@pwr.edu.pl (U. Bazylińska).

https://doi.org/10.1016/j.colsurfb.2025.114754
Received 17 January 2025; Received in revised form 12 April 2025; Accepted 28 April 2025
Available online 30 April 2025

makes them exceptionally well-suited for use in Photodynamic Therapy (PDT), a technology that requires the activation by light of a photosensitizing agent to produce ROS [5]. Since these ROS can selectively target and damage cancerous tissues, PDT is considered as a powerful and effective treatment option for cancer.

In this study, *Ulva rigida* C. Agardh, 1823 (hereafter *U. rigida*), a green marine alga widely distributed in many oceans and seas, also present in the Mediterranean Sea [6], is highlighted as a valuable natural source of chlorophylls. Belonging to the phylum of Chlorophyta (green algae), and known as "sea lettuce", the genus *Ulva* includes more than 400 species worldwide, which often show large biomasses, especially in eutrophic and N-rich shallow coastal environments [7]. In those environments, especially in summer *Ulva* spp can grow exponentially and can suffocate the benthos, thus influencing negatively local fisheries and aquaculture. The *Ulva* spp. widespread presence, easy accessibility and the need to remove their large biomass to avoid any impact on the local economies make them an excellent resource for extracting photoactive compounds, ideal for use in PDT [8]. Because of their rapid growth and easiness of culturing, such algae have also been used for the production of food amendments and biofuel [9,10].

Various techniques have been developed for extracting natural compounds from biomass. However, these methods pose several challenges, being time-consuming, costly, and lacking in environmental sustainability. Consequently, there is a pressing need for more affordable, efficient, and eco-friendly extraction methods. Such advancements would enhance the practical application of these processes and add value to raw materials that are currently underutilized in significant quantities. In this context, Microwave-Assisted Extraction (MAE) is appreciated due to high extraction efficiency, short processing time, and low costs compared to traditional methods [11].

Natural photosensitizers derived from algae are gaining attention in medical and environmental applications due to their biocompatibility and potential therapeutic properties. These photosensitizers, such as chlorophylls, carotenoids, and phycobiliproteins, are naturally occurring pigments found in various algae species. They can be used in photodynamic therapy (PDT) for cancer treatment, where they generate reactive oxygen species upon light activation to target and destroy cancer cells. Algal photosensitizers offer an eco-friendly and renewable alternative to synthetic compounds, with the added benefit of being non-toxic and easily biodegradable [12,13]. Still, several factors limit the clinical use of photosensitizers (PSs). Notably, these compounds are often hydrophobic, leading to aggregation in biological biofluids, and they can degrade when exposed to biological environments. However, these challenges can be addressed by encapsulating PSs within biocompatible nanocarriers. Therefore, the special novelty of our study is focused on exploring the special potential of lipid-based liquid crystalline nanocarriers, known as cubosomes, for the encapsulation, delivery, and release of a newly obtained *Ulva rigida* extract rich in photoactive chlorophylls. Indeed, cubosomes offer a promising solution to enhance the stability and effectiveness of the chlorophyll extract for photodynamic therapy (PDT).

Cubosomes have honeycomb-like nanostructure consisting of a lipid bilayer folded in space and separating two continuous, but not-interconnected water channels [14]. Cubosome-loaded compounds are protected against degradation in solution, and their bioavailability and cellular uptake are largely improved than their free form [15]. These lipid liquid crystalline nanocarriers, moreover, are ideal candidates due to their high colloidal stability, entrapment efficiency, and ability to encapsulate hydrophobic compounds [16]. Commonly, they are stabilized by block copolymers such as Pluronics but other options have been reported to increase their biodegradability [17] and biocompatibility [18,19]. Recently, we have developed and optimized monoolein-based cubosomes and hexosome formulations stabilized by Span 80 and sodium taurocholate [20]. Such formulations, mostly with cubic phases, coloaded with a second-generation PS and an adjuvant, showed good results in PDT applications against skin melanoma cells with minimal cytotoxicity against healthy cells. Herein, the photoactive *U. rigida* extract was encapsulated within standard Pluronic-stabilized cubosomes (CUB) and the new type, less cytotoxic, Pluronic-free cubosomes stabilized by the combination of bile salt and a surfactant (TS-CUB), to tests its delivery, release and phototoxic activity into pancreatic tumor cells BxPC-3. Indeed, pancreatic cancer is one of the leading causes of cancer-related deaths in developed countries [21], primarily due to its complex and challenging treatment. The prognosis is often poor, with only about 9 % of patients surviving beyond five years after diagnosis [22]. Furthermore, pancreatic cancer is considered extremally resistant due to its complex and obstructive tumor microenvironment [23]. Consequently, due to the unique stability and permeability properties induced by the presence of bile salt molecules, encapsulation into the novel cubosomes may be useful as third-generation [24], combining the most promising photosensitizers with modern drug carriers, of effective photosensitizers in PDT.

2. Experimental

2.1. Materials

The molecular building block used for cubosomes preparation was glycerol monooleate (1-monooleoylglycerol, MO, RYLO MG 19 PHARMA, 98.1 wt%), kindly provided by Danisco A/S (Denmark). Other components of the cubosomes were Pluronic F108 (PF108, block copolymer, the stabilizer used in CUB), Span 80 (Sp80, sorbitan monooleate, steric stabilizer in TS-CUB), and taurocholic acid sodium salt hydrate (TC, Taurocholate, bile salt used in TS-CUB). 9,10-anthracenediyl-bis(methylene)dimalonic acid (ABMDMA) for the evaluation of the ROS and $^1O_2$ generation efficiency were purchased from Sigma-Aldrich (Germany; New Zealand). The solvents used in the extraction process (ethanol ≥99.8 %, hexane ≥97.0 %,) were purchased from Honeywell (Germany). Anhydrous sodium sulfate as a drying agent, was purchased from Sigma-Aldrich (Italy).

Acetonitrile and methanol were of HPLC grade and were purchased from Sigma-Aldrich (Italy). Orthophosphoric acid (ACS ISO, for analysis, 85 %) was purchased from Carlo Erba Reagents S.r.l. (Italy).

Water was freshly distilled and filtered through a Milli-Q apparatus (Millipore, Italy) and is referred to as water (W). For the preparation of the cubosomes, the water was filtered (before preparation) with a 0.22 μm pore size hydrophilic filter (Milli-Q system by Millipore, Germany). The analytical standards of lutein, chlorophyll a, and chlorophyll *b* were purchased from Sigma-Aldrich (Italy).

2.2. Biomass collection and preparation

Fresh *U. rigida* marine algae were collected from the Mediterranean Sea in Sardinia (Italy). The algae were washed with water to remove sand, salt, and epiphytes, deep-frozen at -80 °C, and freeze-dried (Benchtop, VirTis, US) for 48 h. The dry weight of the algae was 12.89 % of the fresh biomass. Then, the freeze-dried algae were milled into powder using a ball-milling technique to increase the extraction surface. For this purpose, the freeze-dried *Ulva rigida* (1.5 g) was loaded into a zirconium oxide grinding jar (35 mL) equipped with two balls (ϕ = 8 mm). The jar was sealed and shaken for 15 min at a frequency of 20 Hz using a VWR® Beater Mixer Mill apparatus. The powdered biomass was then stored in the fridge and used in the following steps.

2.3. Extraction

The bioactive pigments (chlorophylls) were extracted from the powdered biomass as follows (Fig. 1). The extraction was performed in a two-steps process including solid-liquid microwave-assisted extraction and liquid-liquid extraction with pigments fractionation in a separatory funnel.

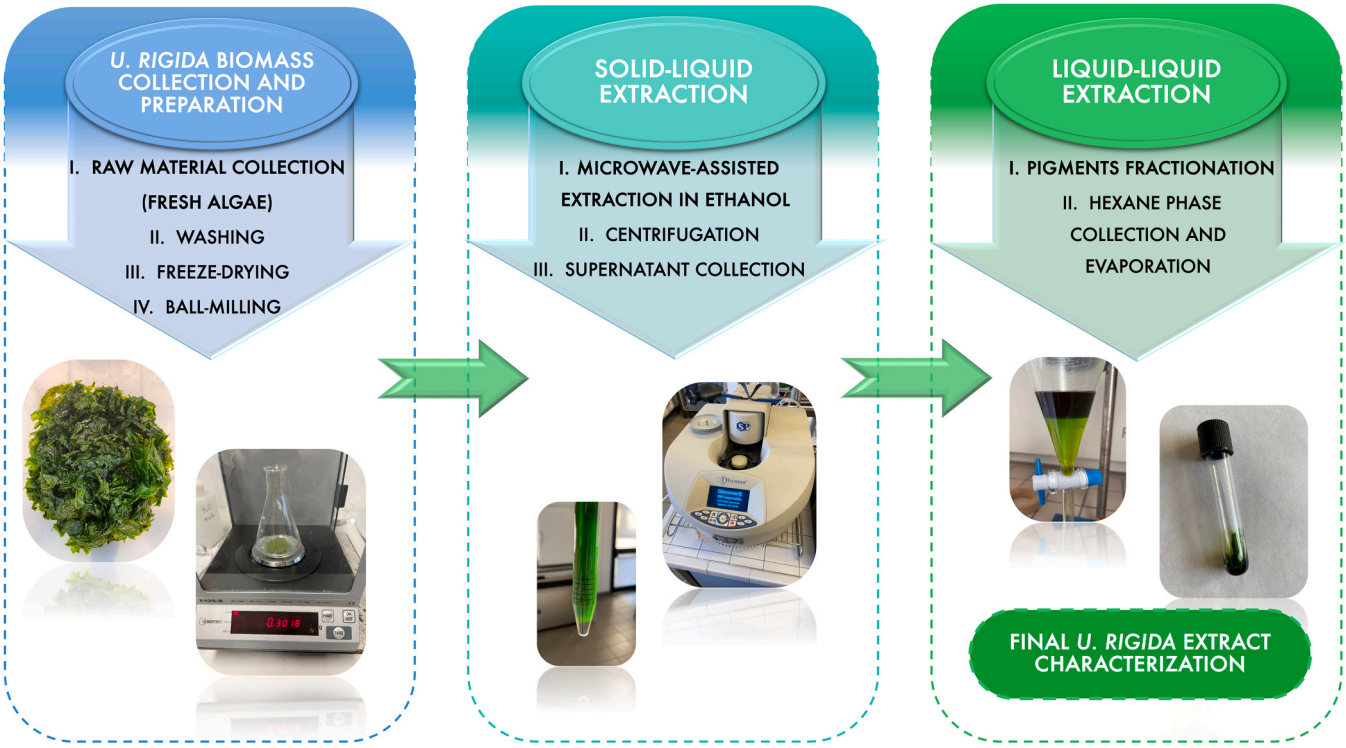

Fig. 1. General scheme of the pigments extraction process from *U. rigida* marine algae biomass.

2.3.1. Microwave-assisted extraction

To release bioactive compounds from the cell wall into the solvent solution, a solid-liquid extraction was performed using MAE technique (Discover SP, CEM). Ethanol was chosen as a solvent (in a solid-liquid ratio of 0.01 g of dry algae/mL of solvent) since it is a green solvent and gives high efficiency in pigments extraction from *U. rigida* [8]. The biomass was subjected to extraction at 35 °C for 1 min with a power of 300 W and a pressure of 300 PSI. After that, the solution was centrifugated (4000 rpm/10 min) (REMI R-9M, Remi Elektrotechnik Ltd., Indie) and the supernatant was fractionated by liquid-liquid extraction in a separatory funnel for the system composed of 50 % ethanolic extract, 30 % of hexane and 20 % of water, based on the high pigments extraction efficiency obtained in this way by Martins et al. in 2021 [8]. The organic hexane phase, rich in hydrophobic pigments of interest, i.e., chlorophylls, was collected, dried with anhydrous sodium sulfate (residual water remove), evaporated, and concentrated under reduced pressure in rotavapor (BÜCHI R-200, BÜCHI Labortechnik AG, Switzerland) giving the final crude *U. rigida* extract used in the next steps.

2.3.2. High-performance liquid chromatography – mass spectrometry – extract qualitative assessment

A qualitative investigation of *U. rigida* extract was performed by an ion mobility QTOF LC-MS system using a 1290 Infinity II UPLC equipped with an autosampler (G7167B), a quat pump (G7120A), a column comp (G7116B) and 6560 IM-QTOF (Agilent Technologies Inc., Palo Alto, CA, US). Before analysis, the instrument performances were tested using an Agilent tuning solution mix (G1969–85000). During the analysis, two reference masses at *m/z* 112.9855 and *m/z* 966.0007 were continuously infused into the system for constant mass correction. Positive electrospray ionization (ESI) ion mode was used to perform all the experiments with the following optimized source parameters: drying gas at 300 °C with a flow of 5 L/min, sheath gas at 350 °C at a flow rate of 12 L/min, nebulizer at 35 psi, capillary voltage set to 3500 V with a nozzle voltage of 500 V. The mass spectra were acquired by full range acquisition covering the *m/z* range of 100–1050.

Chromatographic separation was performed on a Kinetex EVO C18 column (150 × 2.1 mm, 1.7 µm 100 Å, Phenomenex, Castel Maggiore, Bologna, Italy) maintained at 30 ± 1 °C. Isocratic elution of the mobile phase, with a combination of solvent A (0.1 % formic acid) 10 % and solvent B (acetonitrile + 0.1 % formic acid) 90 %, was kept for 30 min at a flow rate of 0.3 mL/min. The injection volume was 4 µL.

Data acquisition and processing were done using MassHunter Workstation Acquisition software v. B.09.00 and MassHunter Workstation Qualitative Analysis software v. 10.0 (Agilent Technologies, Santa Clara, CA, US).

2.3.3. High-performance liquid chromatography – UV-Vis spectroscopy – extract quantitative assessment

The content of pigments in *U. rigida* extract was quantified by high-performance liquid chromatography coupled with an UV-Vis detector (HPLC-UV-Vis).

The HPLC determination was performed according to a previously reported method [25]. Briefly, the analysis was performed by using an Agilent HPLC 1100 liquid chromatograph coupled with a Thermo Finnigan DAD Chromquest UV 6000 diode array detector. The chromatographic analyses were performed by injecting 10 µL of extract solubilized in methanol into a Kinetex column (5 u, C18, 100 A; Phenomenex, Torrance, CA, USA), and eluting with a mobile phase consisting of 0.22 M H_3PO_4 and acetonitrile mixed on a gradient mode. Three wavelengths were used: 430 nm, 470, and 660 nm for chlorophyll *b*, lutein, and chlorophyll a determination, respectively. Peak identification was carried out by comparing each compound's retention time and UV spectrum with the reference standard. Individual compounds were quantified using an external standard calibration method. Correlation values ranged between 0.9990 and 0.9999. The calibration curve (1–10 mg/L) was prepared in methanol from suitable dilution of standard stock solution (1000 mg/L in methanol). All analyses were conducted in triplicate and the data are reported as average value ± standard deviation (SD).

2.4. Cubosome formulations preparation and encapsulation

Cubosome formulations were prepared by following our previously reported methodology [20]. Firstly, MO was melted at 40 °C, then the *U. rigida* extract was added and mixed with the lipid phase, until homogeneous mixing. After that, a water (W) solution of PF108 (CUB) or TC and Sp80 (TS-CUB) was added to the lipid phase and immediately sonicated by an ultrasonic processor (UP100H, Hielscher Ultrasonics, Germany) in 2 cycles (2 and 3 min) with amplitude 90 % with the pulse ON for 1 s followed by 1 s of break. The empty cubosomes were prepared in the same way without the addition of the extract. The composition (wt%) of empty and loaded formulations was MO/PF108/W= 3.3/0.3/96.4 and MO/TC/Sp80/W= 3.5/0.2/0.1/96.2 for CUB and TS-CUB, respectively.

2.5. Dialysis and encapsulation efficiency of the formulations

After encapsulation of the extract of *U. rigida*, the formulations were dialyzed to remove the excess extract into a tubing cellulose membrane (14 kDa of cutoff; Sigma Aldrich), in 2 L of water at room temperature for 2 h, changing the water after 1 h.

The values of encapsulation efficiency (EE) were evaluated via UV-Vis spectroscopy. Absorption spectra were acquired using a UV-Vis spectrophotometer (Cary Series UV-Vis-NIR Spectrophotometer, Agilent Technologies, UK) using quartz cuvette (optical path: 1 cm). In order to calculate the weight of the encapsulated extract before and after dialysis, the standard calibration curve of the extract was prepared, and the data fitted to a linear regression ($R^2 = 0.9993$). Absorption spectra of the cubosome formulations before and after dialysis were measured after dissolving in ethanol (dilution 1:15 v/v) and the EE was obtained through the following equation:

$$EE[\%] = \frac{weight\ of\ the\ extract\ after\ dialysis}{weight\ of\ the\ extract\ before\ dialysis} \times 100$$

2.6. Small-angle X-ray scattering (SAXS)

The structure of the loaded and unloaded formulations was evaluated by means of small angle X-ray scattering (SAXS). The SAXS characterization was performed following our previously published protocol [18,26]. Briefly, the samples were placed in quartz capillaries and measured at a sample to detector distance of 360 mm for around 2 h per sample at a given temperature. The inter-crystalline spacing, d, was calculated after evaluating the q positions of each peak in SAXS pattern using the following equation:

$$d = \frac{2\pi}{q_{peak}} \quad (1)$$

Then, the lattice parameter, a, describing the crystalline unit of the inverse bicontinuous cubic phases was extrapolated from equation 2:

$$a = d \bullet \sqrt{h^2 + k^2 + l^2} \quad (2)$$

Where h, k and l are the Miller's indexes. Finally, the water channel radius of the cubosomes and sponge nanoparticles was evaluated by applying equation 3 and 4, respectively:

$$r_w = (a - l) \bullet \sqrt{\frac{A_0}{-2\pi\chi}} \quad (3)$$

$$r_{w-L3} = \frac{d_{L3}}{d_{cubic}} r_{w-cubic} \quad (4)$$

where χ and A_0 are, respectively, the Euler characteristic and the surface area of the specific geometry (Pn3m, $\chi = -2$, $A_0 = 1.919$), and l is the MO hydrophobic chain length at 25 °C (17 Å) [27].

2.7. Dynamic and electrophoretic light scattering

Dynamic light scattering (DLS) measurements were performed on the diluted (1:50 v/v) samples at 25 °C and 37 °C using a ZetaSizer Nano ZS by Malvern Instruments (Malvern, UK) (backscattering angle 173°, with a 4 mW He-Ne laser at 632.8 nm). All measurements were conducted in triplicate and the data are reported as average value ± standard deviation (SD). The apparent hydrodynamic radius (D_h) and polydispersity index (PdI) were extracted by a second-order cumulant analysis. The ζ-potential was evaluated using electrophoretic light scattering (ELS) by applying the Smoluchowski equation to the electrophoretic mobility.

2.8. Cryogenic transmission electron microscopy (cryo-TEM)

The morphology of the formulations under investigation was studied using cryogenic transmission electron microscopy following the usual protocol for liquid crystalline nanoparticles employed by our group [18]. The sample (4 μL) was blotted on the grid at 25 °C with a relative humidity of 90 %, within 24 h from preparations and imaged using a Jeol JEM-2200FS transmission electron microscope (JEOL, Tokyo, Japan).

2.9. Reactive oxygen assay

Experiments are based on the reaction $^1O_2$ with the scavenger molecule 9,10-anthracenediyl-bis(methylene)dimalonic acid (ABMDMA). Singlet oxygen causes ABMDMA photooxidation, resulting in a decrease of the absorbance. Spectrophotometric measurements of each sample using a UV-1650PC UV-Vis Spectrophotometer (Shimadzu, Japan) were performed for 1 h by evaluating the ABMDMA (0.15 mM) absorbance at 401 nm every 0, 1, 3, 6, 9, 12, 16, 20, 25, 30, 35, 40, 45, 50, 55, 60 min. The ABMDMA absorbance % was calculated for each sample.

2.10. Biological activity

2.10.1. Cell lines

The BxPC-3 cells (human pancreatic cancer cell lines, CRL-1687), purchased in ATCC®, were derived from a 61-year-old female in 1986. The cells were maintained in culture flasks with a surface area equal to 75 cm^2 (Falcon® Cell Culture Flasks) in DMEM (IITD, Wroclaw, Poland) supplemented with 10 % fetal bovine serum (FBS) and 50 μg/mL penicillin and streptomycin (Sigma-Aldrich, Poznan, Poland). The cultures were incubated in a humidified atmosphere with 5 % CO_2 at 37 °C. The cells used for all experiments were detached by trypsinization (Trypsin-EDTA solution) and neutralized with Dulbecco's Phosphate Buffered Saline (DPBS), which was purchased from Sigma-Adrich (Poznan, Poland).

2.10.2. Cytotoxicity studies

The cytotoxicity MTT (3-(4,5-dimethylthiazol-2-yl)-2,5-diphenyl tetrazolium bromide) cell proliferation assay (Sigma-Aldrich, Poznan, Poland) was performed at different extract concentrations (0.17, 0.34, 0.88, 1.3, 1.7, 2.6, 5.2 μg/mL) on the BxPC-3 cell line, after 24 h of incubation in dark conditions with CUB and TS-CUB loaded with the extract, as well as empty CUB and TS-CUB, and free extract. The loaded formulations were diluted to obtain a given extract concentration for the MTT test. During this process, along with the dilution of the extract inside the nanocarriers, the samples CUB/TS-CUB were also diluted, hence also the main component of each formulation, MO namely. Therefore, to compare empty and loaded nanocarriers with the same MO concentration for a given extract concentration (indicated on the x-axis in Fig. 4), all formulations were diluted in the same manner. Therefore, the extract concentrations used in the study correspond to 15.4, 30.8, 77.0, 116, 154, 231, 462 μg/mL of the MO concentration in CUB, and

16.2, 32.4, 81.0, 122, 162, 243, 486 μg/mL in TS-CUB. Generally, 200 μL of cells (approximately 2×10^5 cells) were placed into 96-well plates (Sarstedt, Equimed, Wroclaw, Poland). Cell viability in each test group was expressed as percentages of the control cells (untreated with studied samples). Then, the absorbance was measured at 560 nm using a GloMax® Discover Microplate Reader (Promega) allowed us to evaluate the cell viability in each group. All experiments in this study were conducted in triplicate and the data are reported as average value ± standard deviation (SD).

2.10.3. Cellular uptake and internalization (flow cytometry)

Flow cytometric analysis was performed for the assessment of the ability of BxPC-3 cells to uptake both the formulations loaded with the extract (CUB + extract and TS-CUB + extract).

This technique was applied, due to the well-known fluorescence of the chlorophylls present in the extract, measured by flow cytometer. For this purpose, the cells (density of 4×10^5) were seeded on 24-well plates and left to adhere overnight. Each formulation was added to a final concentration of extract corresponding to 1.3 μg/mL and the cells were incubated for 24 h at 37 °C. Empty nanocarriers (CUB and TS-CUB) were tested as negative controls, due to the lack of fluorescence ability of these samples. After incubation, followed by washing in PBS (not containing calcium and magnesium ions, IITD, Poland), cells were trypsinized and resuspended in 0.5 mL of PBS (BioShop, EPRO, Poland). The flow cytometric measurements were performed on a CyFlow Cube 6 flow cytometer (Sysmex, Poland). The fluorescence of the extract was measured with a FL-5-H detector. 10 000 events were included from each sample. Data were collected and analyzed by CyView software (Sysmex, Poland).

2.10.4. Photodynamic action and immunofluorescent F-actin staining protocol

The photodynamic action of the loaded formulations was evaluated by the immunofluorescence method [28] to evaluate the reorganization of cellular cytoskeleton organization after laser irradiation, applied for red light-activated cubosomes loaded in BxPC-3 cells. Cancer cells were seeded directly on 18 mm diameter round microscope coverslips (Thermo Fisher Scientific Inc.) in 6-well plates (Sarstedt, Equimed, Poland). The cells were left to adhere for 24 h. After this time, the cells were treated with cubosomes for 24 h with a final concentration corresponding to 1.3 μg/mL of the extract. After incubation, samples were irradiated for 5 min using a red-light laser diode (12 mW/cm^2). After washing twice with PBS (BioShop, EPRO, Poland), the cells were fixed for 10 min in 4 % v/v paraformaldehyde (Polysciences, Inc., Bergstrasse, Germany), and washed again with PBS.

The integrity of the cytoskeleton was determined by immunofluorescent labeling of F-actin cells with Phalloidin-iFluor® 488 (Sigma Aldrich, Poznan, Poland). FluorshieldTM with a fluorescent DNA-binding dye of cells grown in the culture (4,6-diamidino-2-phenylindole, DAPI) was used to visualize the nuclei and mount the cells after excitation at 405 nm. Samples were examined on an Olympus BX53 fluorescence microscope (Evident Europe GmbH, Warsaw, Poland).

2.10.5. Statistical analysis

Results of the *in vitro* experiments are presented as mean values ± SD for minimum $n = 3$ and compared by two-way ANOVA for multiple comparisons and $\alpha = 0.05$. Comparisons of samples exhibiting p values ≤ 0.05 and ≤ 0.01 were considered statistically significant and highly significant, respectively. Results were analyzed using the commercial software GraphPad Prism 7.0.

3. Results and discussion

3.1. Characterization of U. rigida extract and encapsulation in the nanocarriers

The extraction of an active component from a biomass is a crucial step that should be as efficient and as green as possible. Microwave-assisted extraction using ethanol was selected for its high efficiency, short processing time, and environmentally friendly approach. This method leverages microwave energy to disrupt the cell walls of algae, releasing the desired pigments into the solvent. Subsequently, the solvent solution is processed to isolate a fraction rich in chlorophylls. The final hydrophobic dark-green extract was obtained from *U. rigida* marine algae as described in paragraph 2.3.1. and then characterized in terms of pigments composition. The average yield was (3.5 ± 0.3)% of the dry algae weight (see section 2.2.). The qualitative HPLC-MS analysis confirmed the presence of chlorophyll in the extract (Figure SI1). The comparison of UV-Vis spectrum and retention time of the analytical standard and sample peaks in HPLC-DAD analysis also highlighted the presence in the extract of chlorophyll *b* and lutein. The content of chlorophyll a and chlorophyll *b* in the extract quantified by HPLC-UV-Vis measurements was (28 ± 4)% and (2.6 ± 0.5)%, respectively, corresponding to (0.98 ± 0.09)% and (0.093 ± 0.008)% of the dry algae weight. A small amount of lutein, (0.92 ± 0.01) %, was also detected in the extract. The UV-Vis spectra of the quantified pigments are presented in Figure SI2.

Cubosome formulations loaded with *U. rigida* extract in a concentration 0.375 mg/mL were obtained with EE equal to (99.2 ± 0.5)% in the case of standard CUB and (97.3 ± 0.9)% for TS-CUB. No significant differences can be highlighted in this case among the conventional and the novel formulations, showing that both nanoparticles can accommodate similar amount of hydrophobic payload in the lipid palisade, as commonly observed in similar formulations [20,29,30]. Verification of the encapsulated extract localization in the hydrophobic part of the cubosome nanocarriers is shown in Figure SI3.

3.2. Physico-chemical characterization of the carriers encapsulating the extracts

SAXS measurements of the formulations containing the extract were performed to evaluate the phase and inner structure at 25 °C and 37 °C and then cooling the sample down to 25 °C again to observe any structural hysteresis. Such temperatures were chosen to study the behavior of the formulations in storage and *in vivo* conditions. These results are shown in Fig. 2 and the lattice parameter (a) and water channel radius (r_w) evaluated from the patterns are presented in Table 1.

In the case of CUB loaded with the extract, only the Pn3m phase could be observed, inferring that the extract interacts with the lipid bilayer of MO. While the two first peaks may be indexed to Pn3m, the subsequent ones are presented at the level of noise, probably related to the presence of vesicles, as observed at the cryo-TEM (Fig. 2C). Nevertheless, in conjunction with cryo-TEM results, we can state that these two peaks are assigned to the Pn3m phase. Indeed, for the standard cubosomes formulated with Pluronics, a biphasic system with a Pn3m + Im3m phase is expected [31], where the former is related to the native structure of MO at this concentration of use in water and the latter is induced due to the interaction of the hydrophobic segment of the block copolymer with the lipid bilayer. The lattice parameter and water channel radius evaluated are in line with those reported in the literature with similar compositions [32,33]. When the temperature is increased to 37 °C, the phase is preserved and only a shift of the peaks at higher q values is noted, decreasing slightly the structural parameters. Cooling down the sample to 25 °C yields the same phase with a small hysteresis as the peak position of the Pn3m is not the same after the treatment. Such a phenomenon could be related to a longer equilibration time (more than 1 h) needed for the Pn3m phase to rearrange in the initial

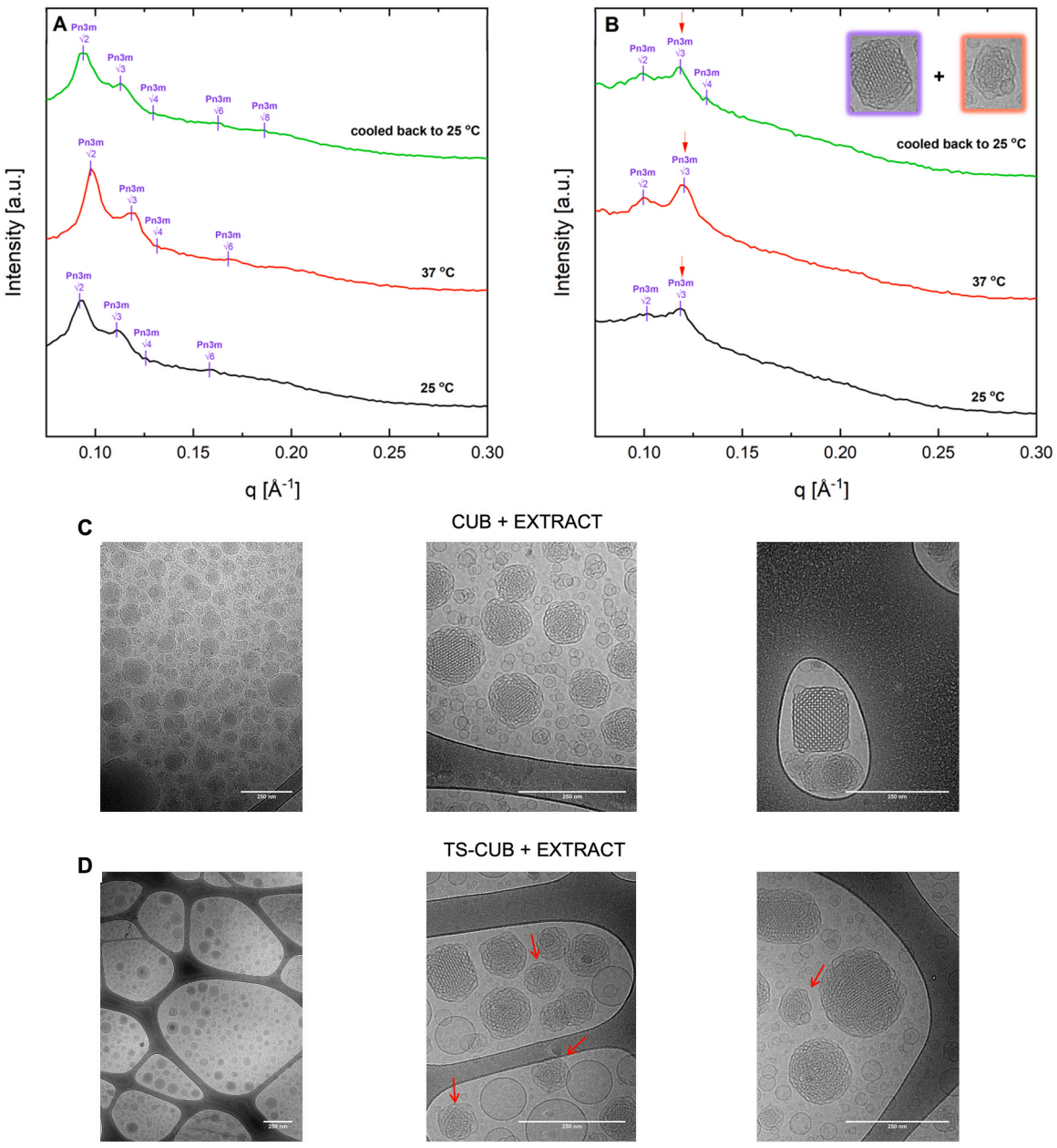

Fig. 2. SAXS diffractograms obtained at 25 °C, 37 °C and then after cooling back to 25 °C of CUB (**A**) and TS-CUB (**B**) loaded with *U. rigida* extract, along with the cryo-TEM images of these samples (**C**) and (**D**), respectively. Red arrows in (**B**) indicate the peak related to the possible presence of an L3 phase, followed by the observation of sponge nanoparticles in (**D**).

Table 1
Phase, lattice parameter (a), and water channel radius (r_w) of the investigated CUB and TS-CUB loaded with *U. rigida* extract measured at 25 °C, 37 °C, and then after cooling back to 25 °C. Data are reported as mean ± SD.

Sample	Temperature (°C)	Phase	a (Å)	r_w(Å)
CUB + extract	25	Pn3m	98 ± 1	21.3 ± 0.6
	37	Pn3m	93 ± 2	19.2 ± 0.8
	back to 25	Pn3m	96 ± 1	20.4 ± 0.4
TS-CUB + extract	25	Pn3m	90 ± 3	18 ± 1
		L3	-	15.5
	37	Pn3m	89.9 ± 0.8	18.1 ± 0.3
		L3	-	15.0
	back to 25	Pn3m	92 ± 3	19 ± 1
		L3	-	16.0

state after the heating and cooling cycle.

In general, the formulation TS-CUB encapsulating the extract shows peaks less intense and less defined, with a higher and broader diffusive band which has been associated with the presence of polydisperse vesicles in the sample [26] (as it will be explained in the next section about the morphology). As already reported by our group, the empty formulation is supposed to be a pure Pn3m. In the case of the formulation loaded with the extract, we observe two visible peaks with positions in line with a Pn3m. However, a second phase may be present in the sample as the second peak is more intense than the first one, and scattering peaks normally decrease with the order of scattering as it is a probabilistic event [34]. Even though this scenario could be related to the alignments of the crystalline planes that may present scattering more intense than the first-order one, it is still probable that the sample is represented by two co-existing phases. Namely, by looking at the phase diagram of MO with other additives, such as Sp80 [35], it is possible to

obtain an L3 phase. Since, in this work, we prepared the nanocarriers with similar lipid composition and Sp80 as well, an analogous phase behaviour can be predicted, namely closer to the border between the Pn3m and L3 phases. Therefore, when compared with the cryo-TEM images of this formulation (Fig. 2D), the scenario of the occurrence of the second phase (L3) is more likely to occur, because structures resembling sponge particles are visible, as indicated by the red arrows. Moreover, Sp80 may tune the lipid (commonly, MO or glycerol monooleate) packing parameter and originate a more disordered cubic phase, commonly referred to as L3 or sponge phase [35]. Usually, a sponge phase exhibits two diffusive bands [36,37], being the first related to cell-cell interaction and the latter to the bilayer thickness. It could be speculated that the peak positioned at $q = 0.12$ Å^{-1} may be linked to the cell-cell interaction in such structure. The heating to 37 °C makes the peaks of the Pn3m and the first of the L3 phase more pronounced, and the shift towards higher *q* values means that the lattice parameter and water channel radius are decreasing in size. Overall, it can be concluded that encapsulation of *U. rigida* extract influences the nanostructure of both types of nanoparticles, by changing the effective packing parameter of MO. Given that drug release is directly linked to the internal structure of the nanocarrier, it is crucial to consider this aspect, particularly in the case of TS-CUB, due to the presence of nanoparticles characterized by an L3 phase.

As a final remark, it can be noticed that the formulations are not temperature-responsive, proving that body temperature does not affect the nanoparticles' structure.

Cryo-TEM measurements were then performed to assess the morphology of the nanoparticles (Fig. 2C and D). Starting with the CUB formulation loaded with the *U. rigida* extract, reported in Fig. 2C, the typical honeycomb-like structures of cubosomes are observed [16,38]. Small vesicles are also highlighted, very likely due to the presence of Pluronic in the sample, which affect the original curvature of the lipid interface [39]. The TS-CUB formulation loaded with the *U. rigida* extract shows three kinds of nanoparticles (Fig. 2D): (i) vesicles of different sizes in the range 20–200 nm, whose presence can be explained by the different curvature of the interface induced by the TC [26], (ii) cubosomes displaying the same morphology and inner structure as reported for the CUB sample, and (iii) sponge nanoparticles (indicated with red arrows in the images). The latter case is in line with the data reported in the literature for a sponge phase dispersion with similar compositions [37] and corroborates the SAXS data analysis of the previous paragraph.

Finally, the apparent hydrodynamic diameter (D_h), polydispersity index (PdI) as well as the ζ-potential of the two formulations loaded with *U. rigida* are reported in Table 2 at two different temperatures. Such values are similar to those of empty formulations with similar composition [40]. The increase in temperature does not have a significant impact on the size, however a drop in the absolute values of the ζ-potential is highlighted. This could be due to the higher thermal motion of the ions at the interface, yielding a lower-charged double layer surrounding the nanoparticles. The size distributions are not affected by the temperature increase and are in line with the ones of cubosomes and sponge phase nanoparticles [35,41]. Moreover, the stability in time of the given formulations was demonstrated by 2 months lasting experiment (Figure SI4).

Table 2
Apparent hydrodynamic diameter (D_h) of the nanoparticles, Polydisperisty Index (PdI) and electrophoretic mobility (ζ-potential) of CUB and TS-CUB formulations loaded with *U. rigida* extract at 25 °C and 37 °C. Data are reported as average value ± SD.

	T (°C)	CUB + extract	TS-CUB + extract
D_h (nm)	25	133 ± 1	114 ± 1
	37	131 ± 1	120 ± 1
PdI	25	0.128 ± 0.005	0.189 ± 0.009
	37	0.13 ± 0.01	0.19 ± 0.02
ζ-potential (mV)	25	- 26 ± 3	- 41 ± 2
	37	- 19.1 ± 0.4	- 32 ± 1

3.3. ROS production

The evaluation of ROS is shown in Fig. 3, where CUB and TS-CUB loaded with *U. rigida* extract as well as the pure extract are compared at different concentrations of the extract (0.88, 1.7, 3.4, 5.2 and 8.8 μg/mL). All samples exhibit the ability to generate ROS, as the % of remaining ABMDMA decreases with time in all cases, proving their photosensitive activity. The strongest ROS production was observed for TS-CUB loaded with extract at the highest concentration (8.8 μg/mL), since the presence of scavenger decreased from 100 % to (85 ± 2)% after 1 h. In contrast, the weakest ROS generation was presented in the case of pure extract of the same concentration, showing (98 ± 2) % of remaining ABMDMA.

Such counterintuitive behavior could be related to the aggregation or degradation of the pigment when not protected by encapsulation in the lipid carriers. Inversely, increasing the concentration of the extract, either encapsulated in CUB or TS-CUB, induces a stronger photoactive effect. Previous studies also reported an increase in ROS generation for other lipid nanocarriers loaded with a photosensitizer as its concentration increased [28,42]. In general, it can be stated that the activity of the extract within the formulation is higher than the one of the free forms, inferring that the encapsulation enhances the photosensitivity following the ROS production.

3.4. Biological activity

3.4.1. Cytotoxicity evaluation

The cytotoxicity MTT test on human pancreatic cancer cell line (BxPC-3) was performed at different extract concentrations (0.17, 0.34, 0.88, 1.3, 1.7, 2.6, 5.2 μg/mL), after 24 h of the cells' incubation in dark conditions. According to ISO 10993–5, cell viability under 80 % is considered as cytotoxic effect, divided into weak (80 % – 60 %), moderate (60 % – 40 %), and strong (below 40 %) cytotoxicity [43]. The results presented in Fig. 4 show the viability of BxPC-3 cells treated with the studied samples of empty CUB and TS-CUB (prepared in the same manner as the loaded nanocarriers, to achieve the given extract concentration, indicated on the x-axis, as described in the Experimental section), the free *U. rigida* extract, and the CUB and TS-CUB loaded with the extract.

In case of the sample with the free extract, the cell viability tends to decrease while increasing its concentration. Pure extract shows the most significant reduction in cell viability, with a drop to approximately 40 % at 5.2 μg/mL. However, when comparing the sample with loaded extract and empty cubosomes, it can be observed that the composition of empty nanocarriers also plays an important role in cytotoxicity due to the possible cytotoxic effect of MO and Pluronic [44,45], especially in case of the 2.6 μg/mL. The lowest viability is observed at the highest concentration (5.2 μg/mL) for all groups. It can be noticed a concentration dependence where at lower concentrations (0.17–1.3 μg/mL), all treatments show a minimal reduction in cell viability, with values remaining close to the control level. However, as the concentration increases beyond 1.7 μg/mL, the cytotoxic effect becomes more pronounced. Significant cytotoxic effects and differences between the various samples become evident at the extract concentration of 2.6 μg/mL. At this dose, the new cubosomes (TS-CUB) exhibit no notable toxicity, in contrast to the standard formulation (CUB), which shows moderate cytotoxicity. This observation indicates that cytotoxicity is reduced when cubosomes are stabilized with TC and Sp80 instead of PF108, supporting the improved biocompatibility of the new formulation. Upon loading the cubosomes with the extract, an increased cytotoxic effect is observed: moderate for CUB + extract and weak for TS-CUB + extract. This effect is likely related to the extract itself, as a weak cytotoxic response is also observed for the extract in its free form at this concentration. Notably, in the case of the standard Pluronic-based

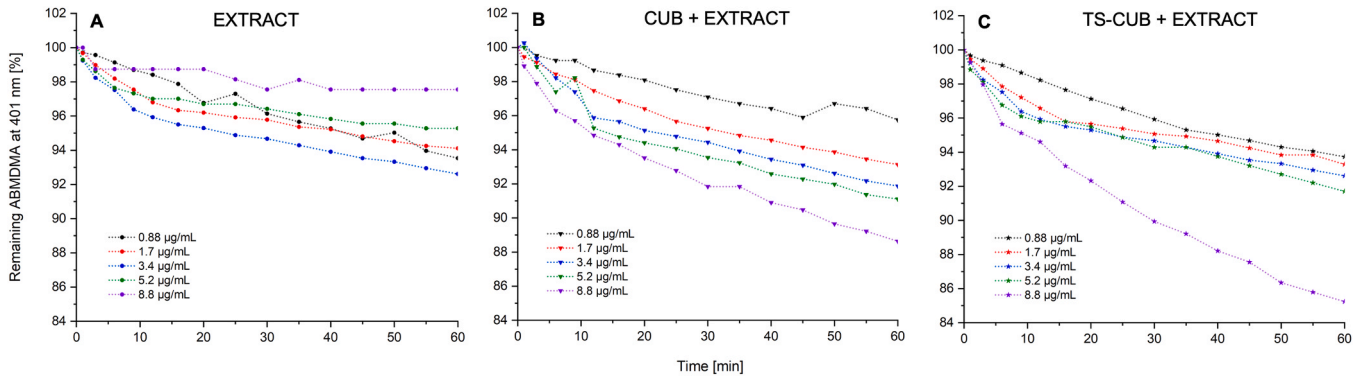

Fig. 3. Photo-oxidation of ABMDMA with the extinction of its absorbance by $^1O_2$ generated by the studied samples: *U. rigida* extract (**A**), CUB (**B**), and TS-CUB loaded with *U. rigida* extract (**C**) at different concentrations (0.88, 1.7, 3.4, 5.2 and 8.8 µg/mL).

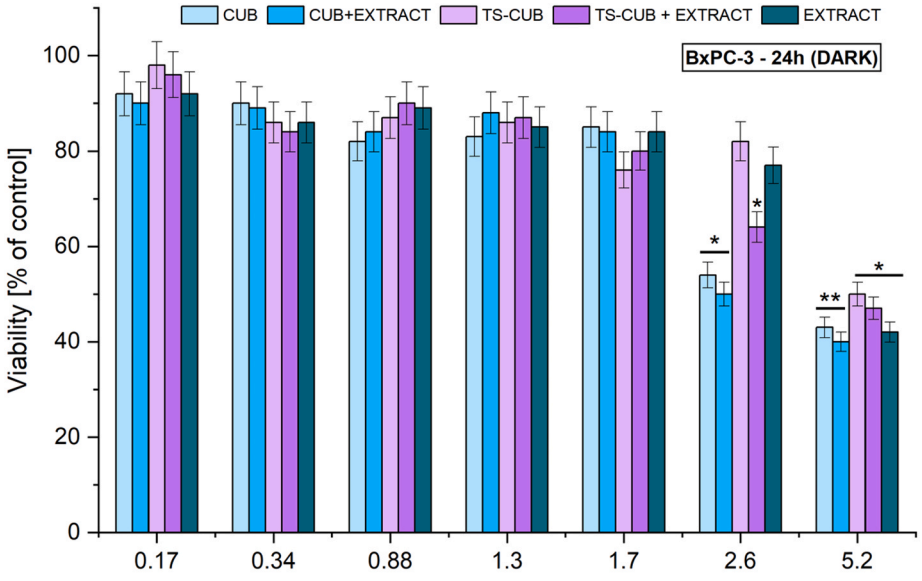

CUB	15.4	30.8	77.0	116	154	231	462
TS-CUB	16.2	32.4	81.0	122	162	243	486

* $p<0.05$
** $p<0.01$

Fig. 4. *In vitro* cytotoxicity experiments: MTT test on BxPC-3 cells after 24 h of incubation with the investigated samples: CUB and TS-CUB loaded with *U. rigida* extract and free extract at different extract concentrations (0.17, 0.34, 0.88, 1.3, 1.7, 2.6, 5.2 µg/mL) compared to empty cubosomes, diluted in the same way as the loaded ones (to the target extract concentration), to achieve comparable MO concentrations in the formulations, indicated below the x-axis for each sample. The results are represented as mean values ± SD for minimum n = 3, * statistical ANOVA analysis: $p \leq 0.05$ and $p \leq 0.01$.

CUB formulation, the cytotoxicity may also be attributed in part to the high monoolein content (231 µg/mL), since both CUB and CUB + extract show comparable levels of toxicity. In contrast, for TS-CUB + extract, the significantly lower cells viability compared to the free extract and the unloaded TS-CUB formulation may reflect the advantages of encapsulation in TS-CUB, such as an enhanced cellular delivery of the extract. The improved efficacy of this formulation will be further explored in the following section on cellular uptake. At 5.2 µg/mL all the samples caused the death of 50 % or more cells, showing that this concentration is unsuitable for medical purposes, related probably to too high concentration of the MO in nanocarriers, as well as too high concentration of the extract itself.

It is worth noting that the literature generally agrees on a cytotoxic threshold for MO-based cubosomes of approximately 100 µg/mL [16,30,44]. Of course, such observed cytotoxicity can vary depending on the stabilizer used (e.g., we observed a 25 % decrease in toxicity when a polyphosphoester analog of PF127 was employed) [18]. Cytotoxicity can also differ based on the specific resistance of the cell line to which the formulation is administered. Particularly, the pancreatic cancer cells utilized in this study are notably resilient, as pancreatic cancer ranks among the most lethal cancers, with one of the lowest survival rates [46,47], and numerous studies were aimed to investigate the underlying mechanisms contributing to this resistance [23,46–49]. This fact may explain why the biocompatibility tests here presented on BxPC-3 cells

under dark conditions showed no significant cytotoxic effect up to a MO concentration of 154 μg/mL, which corresponds to 1.7 μg/mL of *U. rigida* extract. Given this cytotoxicity threshold, samples containing 1.3 μg/mL of *U. rigida* extract were selected for the subsequent assessment of cellular uptake and photodynamic action.

3.4.2. Cellular uptake evaluation

In this study, flow cytometry was used to count cells emitting fluorescence due to specific fluorochromes present within (in this case the fluorescent extract), with the right shifts presented in Fig. 5 indicating higher cellular uptake. Based on these experiments, Fig. 5 evaluates the cellular uptake of the algae extract by BxPC-3 cells treated with various samples. Control cells were compared with cells treated with the free extract (1.3 μg/mL), CUB, and TS-CUB, either loaded with the extract (1.3 μg/mL) or as empty carriers (negative controls).

As expected, fluorescence in control cells and cells treated with empty cubosomes was low and nearly identical, being related only to the autofluorescence emitted by cells [50]. However, a significant increase in fluorescence was observed in cells treated with the pure extract and CUB + extract. An even greater increase was noted in cells treated with TS-CUB + extract. Accordingly, comparison with the controls supports the conclusion that the enhanced cellular uptake of the extract resulted from its encapsulation in the obtained nanocarriers. The observed difference in cellular uptake between the two extract-loaded cubosome formulations, along with their different compositions, suggest that TC and Sp80 may play a role in the higher internalization efficiency of the algae extract when administering the novel cubosomes. The presence of such compounds may further modulate membrane fluidity and permeability, thereby facilitating the internalization process [51]. Another motivation for increased cellular uptake in the case of TS-CUB + extract, can be found in the smaller particle size and more negative ζ-potential of the new cubosomes compared to standard ones, which could facilitate easier transport through the tumor cellular membrane. Indeed, smaller particle size typically enables a more efficient endocytosis process, and a negative ζ-potential can promote stronger electrostatic interactions with positively charged domains on cellular membranes, potentially enhancing internalization [52]. While these suggestions are consistent with existing literature, further mechanistic studies are required to confirm the precise uptake pathways involved. In conclusion, the TS-CUB formulation delivers the photoactive *U. rigida* extract to the pancreatic tumor cells more efficiently.

3.4.3. Bioimaging of the cell morphology

The phototoxic activity was evaluated by cytoskeleton fluorescent staining before and after irradiation. In Fig. 6 is reported the bioimaging of BxPC-3 pancreatic cancer cells treated with CUB and TS-CUB formulations loaded with *U. rigida* extract (1.3 μg/mL) as well as the free extract at the same concentration, performed in dark conditions and after irradiation. The cell morphology revealed a significant difference in the F-actin appearance in the case of TS-CUB + extract after irradiation. In the case of the TC and Sp80-stabilized cubosomes loaded with the algae extract the cytoskeleton is destroyed as significant reorganization and destabilization of F-actin fibers was observed compared to the other samples, including the empty cubosomes. Comparing the cell bioimaging of free extract after PDT with its loaded form, it can be observed that encapsulation, particularly in the case of TS-CUB formulation, significantly enhances the extract's efficacy and photosensitivity.

These results are in good agreement with our previous study concerning the cytoskeleton observation after PDT [38], demonstrate the potency of our formulation in increasing the extract toxicity against pancreatic cancer cells when combined with photodynamic treatment.

4. Conclusions

Due to the increasing death rate and the urgent need for an effective drug to combat resistant pancreatic cancer, we propose a solution based on photoactive algae extracts encapsulated in modern nanocarriers, cubosomes, combined with PDT. As demonstrated in this work, this approach allows the bioactive cargo to be delivered in a stable and bioactive form to targeted cancer cells, even at body temperature

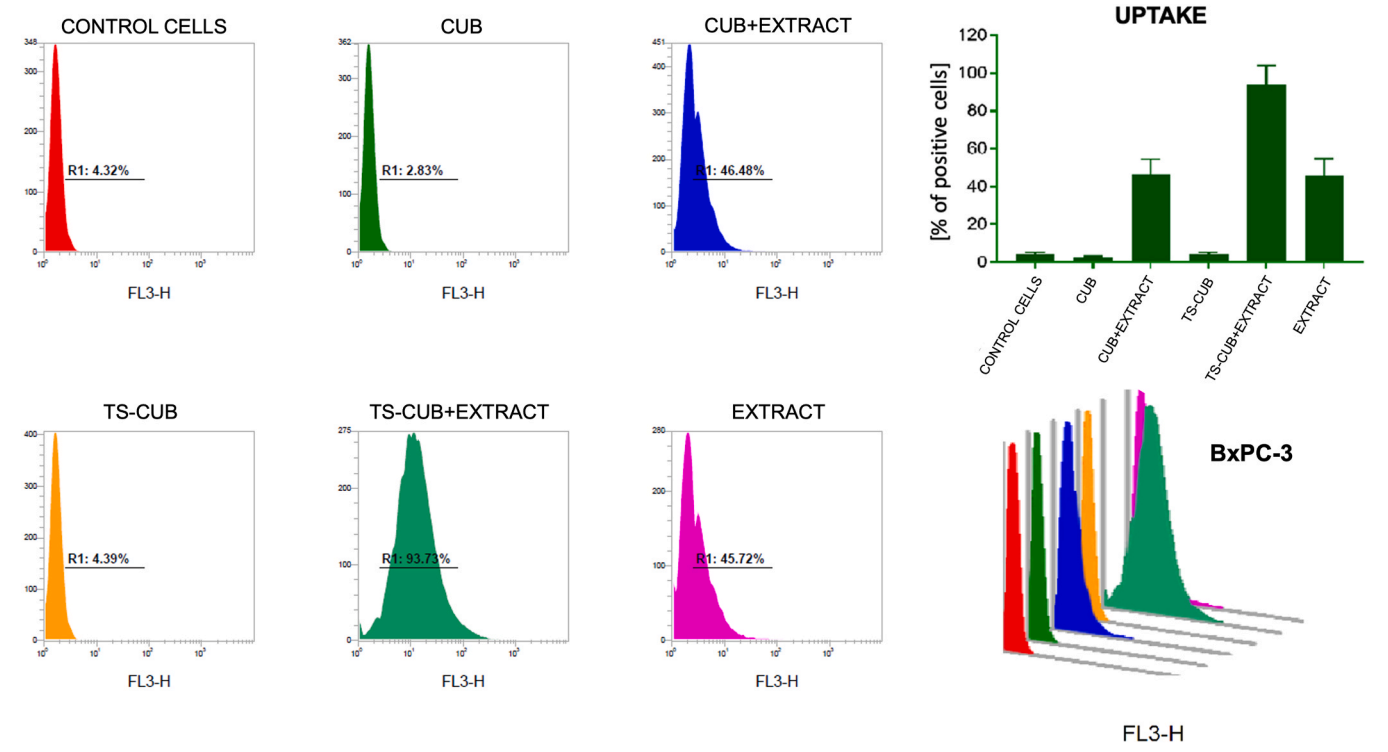

Fig. 5. Flow cytometry experiments on BxPC-3 cells – purpose of the cellular uptake of the studied samples: CUB and TS-CUB loaded with *U. rigida* extract (1.3 μg/mL) compared to free extract (1.3 μg/mL) with three negative controls (empty CUB and TS-CUB, as well as untreated control cells).

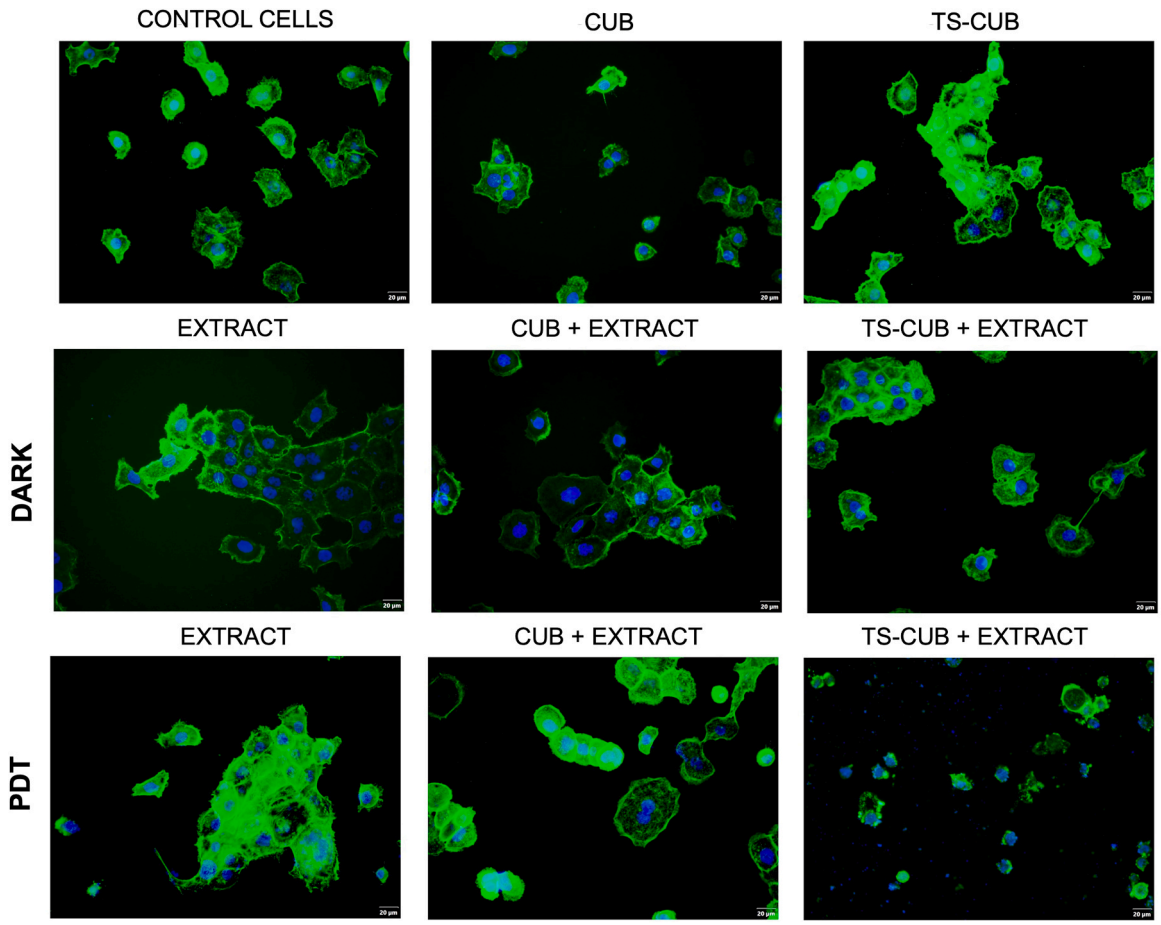

Fig. 6. Bioimaging performed on human pancreatic cancer cell line (BxPC-3) in dark conditions (DARK) as well as after irradiation (PDT); cells were treated with different samples: empty CUB and TS-CUB; extract-loaded (1.3 μg/mL) CUB and TS-CUB, as well as free extract (1.3 μg/mL).

(37 °C), indicating potential *in vivo* applications.

The proposed formulations presented a stable structure. However, apart from the typical Pn3m cubic phase, TS-CUB exhibited possible presence of sponge nanoparticles with an L3 phase. The TS-CUB formulation showcased in this work demonstrated greater photoactivity associated with high ROS production and biocompatibility, characterized by high cellular uptake and reduced cytotoxicity under dark conditions. Nevertheless, upon exposure to irradiation during PDT, these formulations exhibited strong photodynamic anticancer activity, making them ideal candidates for PDT in the treatment of pancreatic cancer.

This work aims to highlight the environmentally friendly development of widely available marine algae biomass, rich in bioactive natural photosensitizers with high photoactivity, enhancing its pharmaceutical value. An additional advantage of the proposed algae extract-based systems is their protection and efficient delivery via cubosome nanocarriers, which offer high stability and loading efficiency. To the best of our knowledge, this is the first work concerning the encapsulation of natural bioactive compounds obtained from marine algae in the cubosomes with increased biocompatibility, thus it may constitute a green template nanoplatform for the research on different valuable compounds obtained from biomass for applications in pharmacy and nanomedicine. In addition, this type of nanocarriers has not been thoroughly studied yet for the potential treatment of highly resistant pancreatic cancer cell line (BxPC-3), especially combined with PDT and natural photosensitizers encapsulation.

CRediT authorship contribution statement

Debora Dessì: Writing – review & editing, Software, Resources, Methodology. **Andrea Porcheddu:** Writing – review & editing, Formal analysis, Data curation. **Rita Mocci:** Writing – review & editing, Methodology, Formal analysis. **Urszula Bazylinska:** Writing – review & editing, Writing – original draft, Supervision, Project administration, Methodology, Investigation, Formal analysis, Conceptualization. **Karolina Krautforst:** Writing – review & editing, Writing – original draft, Visualization, Software, Resources, Methodology, Investigation. **Julita Kulbacka:** Writing – review & editing, Software, Resources, Methodology, Investigation, Formal analysis. **Marco Fornasier:** Writing – review & editing, Software, Resources, Methodology, Investigation, Formal analysis. **Davide Moccia:** Writing – review & editing, Investigation, Formal analysis. **Antonio Pusceddu:** Writing – review & editing, Formal analysis, Data curation. **Giorgia Sarais:** Writing – review & editing, Formal analysis, Data curation. **Sergio Murgia:** Writing – review & editing, Supervision, Formal analysis, Conceptualization.

Declaration of Competing Interest

The authors declare that they have no known competing financial interests or personal relationships that could have appeared to influence the work reported in this paper.

Acknowledgments

UB and KK gratefully acknowledge the support of the National Science Centre (Poland) within a framework of the SONATA BIS 13

program (No. UMO-2023/50/E/ST4/00603) and the Department of Physical and Quantum Chemistry, the Faculty of Chemistry at Wroclaw University of Science and Technology. MF thanks the Division of Physical Chemistry at the Chemical Center for providing access to the Ganesha SAXS instrument and the CHREM imaging facility. SM thanks Fondazione Banco di Sardegna and Regione Autonoma della Sardegna (Progetti Biennali di Ateneo, annualità 2022, CUP F73C23001580007).

Appendix A. Supporting information

Supplementary data associated with this article can be found in the online version at doi:10.1016/j.colsurfb.2025.114754.

Data availability

Data will be made available on request.

References

[1] P.A. Harnedy, R.J. Fitzgerald, Bioactive proteins, peptides, and amino acids from macroalgae, J. Phycol. 47 (2011) 218–232, https://doi.org/10.1111/j.1529-8817.2011.00969.x.
[2] K. Chen, J.J. Ríos, A. Pérez-Gálvez, M. Roca, Comprehensive chlorophyll composition in the main edible seaweeds, Food Chem. 228 (2017) 625–633, https://doi.org/10.1016/j.foodchem.2017.02.036.
[3] B. Pradhan, R. Nayak, S. Patra, B.P. Jit, A. Ragusa, M. Jena, Bioactive metabolites from marine algae as potent pharmacophores against oxidative stress-associated human diseases: a comprehensive review, Molecules 26 (2021), https://doi.org/10.3390/molecules26010037.
[4] V. Rizzi, J. Gubitosa, P. Fini, A. Fraix, S. Sortino, A. Agostiano, P. Cosma, Development of Spirulina sea-weed raw extract/polyamidoamine hydrogel system as novel platform in photodynamic therapy: photostability and photoactivity of chlorophyll a, Mater. Sci. Eng. C 119 (2021), https://doi.org/10.1016/j.msec.2020.111593.
[5] T.J. Dougherty, C.J. Gomer, B.W. Henderson, G. Jori, D. Kessel, M. Korbelik, J. Moan, Q. Peng. REVIEW Photodynamic Therapy, 1998 http://academic.oup.com/jnci/article/90/12/889/960771.
[6] M.D. Guiry, How many species of algae are there? A reprise. Four kingdoms, 14 phyla, 63 classes and still growing, J. Phycol. 60 (2024) 214–228, https://doi.org/10.1111/jpy.13431.
[7] P. Viaroli, M. Bartoli, C. Bondavalli, R.R. Christian, G. Giordani, M. NaldiMacrophyte communities and their impact on benthic fluxes of oxygen, sulphide and nutrients in shallow eutrophic environments, 1996.
[8] M. Martins, R. Oliveira, J.A.P. Coutinho, M.A.F. Faustino, M.G.P.M.S. Neves, D.C. G.A. Pinto, S.P.M. Ventura, Recovery of pigments from Ulva rigida, Sep Purif. Technol. 255 (2021), https://doi.org/10.1016/j.seppur.2020.117723.
[9] S. Lordan, R.P. Ross, C. Stanton, Marine bioactives as functional food ingredients: Potential to reduce the incidence of chronic diseases, Mar. Drugs 9 (2011) 1056–1100, https://doi.org/10.3390/md9061056.
[10] P. Schiener, T. Atack, R.A. Wareing, M.S. Kelly, A.D. Hughes, The by-products from marine biofuels as a feed source for the aquaculture industry: a novel example of the biorefinery approach, Biomass Convers. Biorefin. 6 (2016) 281–287, https://doi.org/10.1007/s13399-015-0190-6.
[11] S.U. Kadam, B.K. Tiwari, C.P. O'Donnell, Application of novel extraction technologies for bioactives from marine algae, J. Agric. Food Chem. 61 (2013) 4667–4675, https://doi.org/10.1021/jf400819p.
[12] E.N. Armendáriz-Mireles, C.A. Calles-Arriaga, W. Pech-Rodríguez, A. Castillo-Robles, E. Rocha-Rangel, Alternative sources of natural photosensitizers: role of algae in dye-sensitized solar cell, Colorants 2 (2023) 137–150, https://doi.org/10.3390/colorants2010010.
[13] X. Bai, W. Liang, J. Sun, C. Zhao, P. Wang, Y. Zhang, Enhanced production of microalgae-originated photosensitizer by integrating photosynthetic electrons extraction and antibiotic induction towards photocatalytic degradation of antibiotic: a novel complementary treatment process for antibiotic removal from effluent of conventional biological wastewater treatment, J. Environ. Manag. 308 (2022), https://doi.org/10.1016/j.jenvman.2022.114527.
[14] R. Varghese, S. Salvi, P. Sood, B. Kulkarni, D. Kumar, Cubosomes in cancer drug delivery: a review, Colloids Interface Sci. Commun. 46 (2022), https://doi.org/10.1016/j.colcom.2021.100561.
[15] Z. Karami, M. Hamidi, Cubosomes: Remarkable drug delivery potential, Drug Discov. Today 21 (2016) 789–801, https://doi.org/10.1016/j.drudis.2016.01.004.
[16] S. Murgia, S. Biffi, R. Mezzenga, Recent advances of non-lamellar lyotropic liquid crystalline nanoparticles in nanomedicine, Curr. Opin. Colloid Interface Sci. 48 (2020) 28–39, https://doi.org/10.1016/j.cocis.2020.03.006.
[17] P. Naidjonoka, M. Fornasier, D. Pålsson, G. Rudolph, B. Al-Rudainy, S. Murgia, T. Nylander, Bicontinuous cubic liquid crystalline phase nanoparticles stabilized by softwood hemicellulose, Colloids Surf. B Biointerfaces 203 (2021), https://doi.org/10.1016/j.colsurfb.2021.111753.
[18] M. Fornasier, S. Biffi, B. Bortot, P. Macor, A. Manhart, F.R. Wurm, S. Murgia, Cubosomes stabilized by a polyphosphoester-analog of Pluronic F127 with reduced cytotoxicity, J. Colloid Interface Sci. 580 (2020) 286–297, https://doi.org/10.1016/j.jcis.2020.07.038.
[19] U. Bazylińska, J. Kulbacka, J. Schmidt, Y. Talmon, S. Murgia, Polymer-free cubosomes for simultaneous bioimaging and photodynamic action of photosensitizers in melanoma skin cancer cells, J. Colloid Interface Sci. 522 (2018) 163–173, https://doi.org/10.1016/j.jcis.2018.03.063.
[20] M. Fornasier, K. Krautforst, J. Kulbacka, P. Jönsson, S. Murgia, U. Bazylińska, Cubosomes and hexosomes stabilized by sorbitan monooleate as biocompatible nanoplatforms against skin metastatic human melanoma, J. Colloid Interface Sci. 677 (2025) 842–852, https://doi.org/10.1016/j.jcis.2024.08.126.
[21] J. Kleeff, M. Korc, M. Apte, C. La Vecchia, C.D. Johnson, A.V. Biankin, R.E. Neale, M. Tempero, D.A. Tuveson, R.H. Hruban, J.P. Neoptolemos, Pancreatic cancer, Nat. Rev. Dis. Prim. 2 (2016), https://doi.org/10.1038/nrdp.2016.22.
[22] R.L. Siegel, K.D. Miller, A. Jemal, Cancer statistics, 2018, CA Cancer J. Clin. 68 (2018) 7–30, https://doi.org/10.3322/caac.21442.
[23] L. Liu, P.G. Kshirsagar, S.K. Gautam, M. Gulati, E.I. Wafa, J.C. Christiansen, B. M. White, S.K. Mallapragada, M.J. Wannemuehler, S. Kumar, J.C. Solheim, S. K. Batra, A.K. Salem, B. Narasimhan, M. Jain, Nanocarriers for pancreatic cancer imaging, treatments, and immunotherapies, Theranostics 12 (2022) 1030–1060, https://doi.org/10.7150/thno.64805.
[24] I.S. Mfouo-Tynga, L.D. Dias, N.M. Inada, C. Kurachi, Features of third generation photosensitizers used in anticancer photodynamic therapy: review, Photodiagnosis Photodyn. Ther. 34 (2021), https://doi.org/10.1016/j.pdpdt.2020.102091.
[25] V. D'amelia, G. Sarais, G. Fais, D. Dessì, V. Giannini, R. Garramone, D. Carputo, S. Melito, Biochemical characterization and effects of cooking methods on main phytochemicals of red and purple potato tubers, a natural functional food, Foods 11 (2022), https://doi.org/10.3390/foods11030384.
[26] M. Fornasier, R. Pireddu, A. Del Giudice, C. Sinico, T. Nylander, K. Schillén, L. Galantini, S. Murgia, Tuning lipid structure by bile salts: hexosomes for topical administration of catechin, Colloids Surf. B Biointerfaces 199 (2021), https://doi.org/10.1016/j.colsurfb.2021.111564.
[27] C.V. Kulkarni, W. Wachter, G. Iglesias-Salto, S. Engelskirchen, S. Ahualli, Monoolein: a magic lipid? Phys. Chem. Chem. Phys. 13 (2011) 3004–3021, https://doi.org/10.1039/c0cp01539c.
[28] D. Wawrzyńczyk, B. Cichy, J.K. Zaręba, U. Bazylińska, On the interaction between up-converting NaYF4:Er3+, Yb3+ nanoparticles and Rose Bengal molecules constrained within the double core of multifunctional nanocarriers, J. Mater. Chem. C Mater. 7 (2019) 15021–15034, https://doi.org/10.1039/c9tc04163j.
[29] M. Fornasier, S. Murgia, Non-lamellar lipid liquid crystalline nanoparticles: a smart platform for nanomedicine applications, Front. Soft Matter 3 (2023), https://doi.org/10.3389/frsfm.2023.1109508.
[30] A. Yaghmur, H. Mu, Recent advances in drug delivery applications of cubosomes, hexosomes, and solid lipid nanoparticles, Acta Pharm. Sin. B 11 (2021) 871–885, https://doi.org/10.1016/j.apsb.2021.02.013.
[31] M. Nakano, T. Teshigawara, A. Sugita, W. Leesajakul, A. Taniguchi, T. Kamo, H. Matsuoka, T. Handa, Dispersions of Liquid Crystalline Phases of the Monoolein/Oleic Acid/Pluronic F127 System, Langmuir 18 (2002) 9283–9288, https://doi.org/10.1021/la026297r.
[32] S. Murgia, S. Bonacchi, A.M. Falchi, S. Lampis, V. Lippolis, V. Meli, M. Monduzzi, L. Prodi, J. Schmidt, Y. Talmon, C. Caltagirone, Drug-loaded fluorescent cubosomes: versatile nanoparticles for potential theranostic applications, Langmuir 29 (2013) 6673–6679, https://doi.org/10.1021/la401047a.
[33] S. Jenni, G. Picci, M. Fornasier, M. Mamusa, J. Schmidt, Y. Talmon, A. Sour, V. Heitz, S. Murgia, C. Caltagirone, Multifunctional cubic liquid crystalline nanoparticles for chemo- and photodynamic synergistic cancer therapy, Photochem. Photobiol. Sci. 19 (2020) 674–680, https://doi.org/10.1039/c9pp00449a.
[34] C.V. Kulkarni, A. Yaghmur, M. Steinhart, M. Kriechbaum, M. Rappolt, Effects of high pressure on internally self-assembled lipid nanoparticles: a synchrotron small-angle x-ray scattering (SAXS) study, Langmuir 32 (2016) 11907–11917, https://doi.org/10.1021/acs.langmuir.6b03300.
[35] M. Valldeperas, M. Wiśniewska, M. Ram-On, E. Kesselman, D. Danino, T. Nylander, J. Barauskas, Sponge phases and nanoparticle dispersions in aqueous mixtures of mono- and diglycerides, Langmuir 32 (2016) 8650–8659, https://doi.org/10.1021/acs.langmuir.6b01356.
[36] J. Gilbert, M. Valldeperas, S.K. Dhayal, J. Barauskas, C. Dicko, T. Nylander, Immobilisation of β-galactosidase within a lipid sponge phase: Structure, stability and kinetics characterisation, Nanoscale 11 (2019) 21291–21301, https://doi.org/10.1039/c9nr06675f.
[37] M. Valldeperas, A.P. Dabkowska, G.K. Pálsson, S. Rogers, N. Mahmoudi, A. Carnerup, J. Barauskas, T. Nylander, Interfacial properties of lipid sponge-like nanoparticles and the role of stabilizer on particle structure and surface interactions, Soft Matter 15 (2019) 2178–2189, https://doi.org/10.1039/c8sm02634c.
[38] U. Bazylińska, D. Wawrzyńczyk, J. Kulbacka, G. Picci, L.S. Manni, S. Handschin, M. Fornasier, C. Caltagirone, R. Mezzenga, S. Murgia, Hybrid theranostic cubosomes for efficient NIR-induced photodynamic therapy, ACS Nano 16 (2022) 5427–5438, https://doi.org/10.1021/acsnano.1c09367.
[39] V. Meli, C. Caltagirone, A.M. Falchi, S.T. Hyde, V. Lippolis, M. Monduzzi, M. Obiols-Rabasa, A. Rosa, J. Schmidt, Y. Talmon, S. Murgia, Docetaxel-loaded fluorescent liquid-crystalline nanoparticles for cancer theranostics, Langmuir 31 (2015) 9566–9575, https://doi.org/10.1021/acs.langmuir.5b02101.
[40] A.M. Falchi, A. Rosa, A. Atzeri, A. Incani, S. Lampis, V. Meli, C. Caltagirone, S. Murgia, Effects of monoolein-based cubosome formulations on lipid droplets and mitochondria of HeLa cells, Toxicol. Res. (Camb.) 4 (2015) 1025–1036, https://doi.org/10.1039/c5tx00078e.

[41] I.D.M. Azmi, S.M. Moghimi, A. Yaghmur, Cubosomes and hexosomes as versatile platforms for drug delivery, Ther. Deliv. 6 (2015) 1347–1364, https://doi.org/10.4155/tde.15.81.
[42] E. Waglewska, I. Maliszewska, U. Bazylińska, Antimicrobial phyto-photodynamic activity inducing by polyphenol-supported Methylene Blue co-loaded into multifunctional bilosomes: advanced hybrid nanoplatform in the skin infections treatment? J. Photochem. Photobiol. B 240 (2023) https://doi.org/10.1016/j.jphotobiol.2023.112650.
[43] ISO 10993-5:2009, Biological Evaluation of Medical Devices. Part 5: Tests for In Vitro Cytotoxicity. International Organization for Standardization, Geneva, Switzerland, 2009.
[44] S. Biffi, L. Andolfi, C. Caltagirone, C. Garrovo, A.M. Falchi, V. Lippolis, A. Lorenzon, P. Macor, V. Meli, M. Monduzzi, M. Obiols-Rabasa, L. Petrizza, L. Prodi, A. Rosa, J. Schmidt, Y. Talmon, S. Murgia, Cubosomes for in vivo fluorescence lifetime imaging, Nanotechnology 28 (2017), https://doi.org/10.1088/1361-6528/28/5/055102.
[45] A. Rosa, S. Murgia, D. Putzu, V. Meli, A.M. Falchi, Monoolein-based cubosomes affect lipid profile in HeLa cells, Chem. Phys. Lipids 191 (2015) 96–105, https://doi.org/10.1016/j.chemphyslip.2015.08.017.
[46] J. Long, Y. Zhang, X. Yu, J. Yang, D.G. Lebrun, C. Chen, Q. Yao, M. Li, Overcoming drug resistance in pancreatic cancer, Expert Opin. Ther. Targets 15 (2011) 817–828, https://doi.org/10.1517/14728222.2011.566216.
[47] S. Chand, K. O'Hayer, F.F. Blanco, J.M. Winter, J.R. Brody, The landscape of pancreatic cancer therapeutic resistance mechanisms, Int J. Biol. Sci. 12 (2016) 273–283, https://doi.org/10.7150/ijbs.14951.
[48] Z. Wang, Y. Li, A. Ahmad, S. Banerjee, A.S. Azmi, D. Kong, F.H. Sarkar, Pancreatic cancer: understanding and overcoming chemoresistance, Nat. Rev. Gastroenterol. Hepatol. 8 (2011) 27–33, https://doi.org/10.1038/nrgastro.2010.188.
[49] M.H. Sherman, G.L. Beatty, Tumor microenvironment in pancreatic cancer pathogenesis and therapeutic resistance, Annu. Rev. Pathol.: Mech. Dis. Annu. Rev. Pathol. Mech. Dis. 18 (2023) 123–148, https://doi.org/10.1146/annurev-pathmechdis-031621-024600.
[50] M. Monici, Cell and tissue autofluorescence research and diagnostic applications, Biotechnol. Annu. Rev. 11 (2005) 227–256, https://doi.org/10.1016/S1387-2656(05)11007-2.
[51] G. Gaynanova, L. Vasileva, R. Kashapov, D. Kuznetsova, R. Kushnazarova, A. Tyryshkina, E. Vasilieva, K. Petrov, L. Zakharova, O. Sinyashin, Self-assembling drug formulations with tunable permeability and biodegradability, Molecules 26 (2021) 6786, https://doi.org/10.3390/molecules26226786.
[52] C. He, Y. Hu, L. Yin, C. Tang, C. Yin, Effects of particle size and surface charge on cellular uptake and biodistribution of polymeric nanoparticles, Biomaterials 31 (2010) 3657–3666, https://doi.org/10.1016/j.biomaterials.2010.01.065.